Important Notice to Authors

Attached is a PDF proof of your forthcoming article in PRA. Your article has 10 pages and the Accession Code is **AT11669**.

Please note that as part of the production process, APS converts all articles, regardless of their original source, into standardized XML that in turn is used to create the PDF and online versions of the article as well as to populate third-party systems such as Portico, Crossref, and Web of Science. We share our authors' high expectations for the fidelity of the conversion into XML and for the accuracy and appearance of the final, formatted PDF. This process works exceptionally well for the vast majority of articles; however, please check carefully all key elements of your PDF proof, particularly any equations or tables.

Figures submitted electronically as separate files containing color appear in color in the online journal. However, all figures will appear as grayscale images in the print journal unless the color figure charges have been paid in advance, in accordance with our policy for color in print (https://journals.aps.org/authors/color-figures-print).

Specific Questions and Comments to Address for This Paper

1 Please see **http://publish.aps.org/authors/solidus-policy-physical-review-a-physical-review-e** and check our change.
2 Please see **http://publish.aps.org/authors/multiletter-symbols-h5** and check our change throughout.
3 Please see multiletter symbols memo and check changes here and throughout.
4 Please check.
5 Please check Ref. [14].
6 Please update Ref. [35] if possible.
FQ: This funding provider could not be uniquely identified during our search of the FundRef registry (or no Contract or Grant number was detected). Please check information and amend if incomplete or incorrect.

Open Funder Registry: Information about an article's funding sources is now submitted to Crossref to help you comply with current or future funding agency mandates. Crossref's Open Funder Registry (https://www.crossref.org/services/funder-registry/) is the definitive registry of funding agencies. Please ensure that your acknowledgments include all sources of funding for your article following any requirements of your funding sources. Where possible, please include grant and award ids. Please carefully check the following funder information we have already extracted from your article and ensure its accuracy and completeness:
National Research Foundation, NRF-CRP12-2013-03

Other Items to Check

- Please note that the original manuscript has been converted to XML prior to the creation of the PDF proof, as described above. Please carefully check all key elements of the paper, particularly the equations and tabular data.

- Title: Please check; be mindful that the title may have been changed during the peer-review process.

- Author list: Please make sure all authors are presented, in the appropriate order, and that all names are spelled correctly.

- Please make sure you have inserted a byline footnote containing the email address for the corresponding author, if desired. Please note that this is not inserted automatically by this journal.

- Affiliations: Please check to be sure the institution names are spelled correctly and attributed to the appropriate author(s).

- Receipt date: Please confirm accuracy.

- Acknowledgments: Please be sure to appropriately acknowledge all funding sources.

- Hyphenation: Please note hyphens may have been inserted in word pairs that function as adjectives when they occur before a noun, as in "x-ray diffraction," "4-mm-long gas cell," and "R-matrix theory." However, hyphens are deleted from word pairs when they are not used as adjectives before nouns, as in "emission by x rays," "was 4 mm in length," and "the R matrix is tested."

  Note also that Physical Review follows U.S. English guidelines in that hyphens are not used after prefixes or before suffixes: superresolution, quasiequilibrium, nanoprecipitates, resonancelike, clockwise.

- Please check that your figures are accurate and sized properly. Make sure all labeling is sufficiently legible. Figure quality in this proof is representative of the quality to be used in the online journal. To achieve manageable file size for online delivery, some compression and downsampling of figures may have occurred. Fine details may have become somewhat fuzzy, especially in color figures. The print journal uses files of higher resolution and therefore details may be sharper in print. Figures to be published in color online will appear in color on these proofs if viewed on a color monitor or printed on a color printer.

- Please check to ensure that reference titles are given as appropriate.

- Overall, please proofread the entire *formatted* article very carefully. The redlined PDF should be used as a guide to see changes that were made during copyediting. However, note that some changes to math and/or layout may not be indicated.

Ways to Respond

- *Web:* If you accessed this proof online, follow the instructions on the web page to submit corrections.
- *Email:* Send corrections to praproofs@aptaracorp.com
    Subject: **AT11669** proof corrections
- *Fax:* Return this proof with corrections to +1.703.791.1217. Write **Attention:** PRA Project Manager and the Article ID, **AT11669**, on the proof copy unless it is already printed on your proof printout.

Characterization of a photon-pair source based on a cold atomic ensemble using a cascade-level scheme

Alessandro Cerè,[1] Bharath Srivathsan,[1,*] Gurpreet Kaur Gulati,[1,†] Brenda Chng,[1] and Christian Kurtsiefer[1,2,‡]

[1]*Centre for Quantum Technologies, National University of Singapore, 3 Science Drive 2, Singapore 117543*
[2]*Department of Physics, National University of Singapore, 2 Science Drive 3, Singapore 117551*

We characterize a source of photon pairs based on cascade decay in a cold ^{87}Rb ensemble. This source is particularly suited to generate photons for interaction with ^{87}Rb based atomic systems. We experimentally investigate the dependence of pair generation rate, single photon heralding efficiency, and bandwidth as a function of the number of atoms, detuning, and intensity of the pump beams. The observed power and detuning behaviors can be explained by the steady-state solution of an established three-level model of an atom. Measurements presented here provide a useful insight on the optimization of this kind of photon-pair source.

I. INTRODUCTION

Time-correlated and entangled photon pairs are an important resource for a wide range of quantum optics experiments, ranging from fundamental tests [1,2] to applications in quantum information [3–5]. A common method to obtain photon pairs is spontaneous parametric down conversion (SPDC) in nonlinear optical crystals [6], which have proven to be extremely useful. However, photons prepared by SPDC typically have spectral bandwidths ranging from 0.1 THz to 2 THz [7,8], making interaction with atomic systems with a lifetime-limited bandwidth on the order of few MHz difficult. Possible solutions to match the bandwidth requirements include the use of optical cavities around the crystal [9–11], filters [12,13], and recently the use of miniature monolithic resonators made of nonlinear optical materials [14]. A different approach uses directly atomic systems as the nonlinear optical medium in the parametric process. There, a chain of near-resonant optical transitions provides an optical nonlinearity that has long been used for frequency mixing in otherwise inaccessible spectral domains. When two of the participating modes are not driven, such systems can be used for photon-pair generation via a parametric conversion process [15–17]. As the effective nonlinearity decays quickly with the detuning from an atomic transition, the resulting photon pairs can be spectrally very narrow.

In this work, we investigate such a photon-pair source based on four-wave mixing in a cold atomic ensemble. The resulting photon pairs are therefore directly compatible with ground-state transitions of ^{87}Rb, and the pair preparation process does not suffer any reduction in brightness caused by additional filtering. This can be interesting for preparing photon states that are fragile with respect to linear losses. A basic description of the source is presented in [18].

This source has already been used, with minor modifications, to obtain heralded single photons with an exponentially rising time envelope [19,20]. We have also studied the amount of polarization entanglement in the generated photon pairs, and observed quantum beats between possible decay paths [21]. The same source has also been used in conjunction with a separate atomic system, a single ^{87}Rb atom trapped in a far off resonant focused beam to study their compatibility [22] and the dynamics of the absorption of single photons by an atom [23]. There, we explored a limited range of experimental parameters, optimized to observe the physical properties of the biphoton state of interest. In this article we present a systematic characterization of the source as function of the accessible experimental parameters. We believe that our scheme is a useful tool for the studies of the interaction of single photons with single and ensembles of atoms. In order to characterize the source, we focus our attention on generation rate, heralding efficiency, and the compromise between rates and bandwidth.

We start with a brief review of the photon-pair generation process, followed by a presentation of the experimental setup, highlighting some of its relevant and differentiating features, and a description of the measurement technique. The rest of the paper covers systematic variations of the source parameters, and their impact on the rates and bandwidth of the emitted photon pairs.

II. FOUR-WAVE MIXING IN COLD ^{87}Rb BASED ON CASCADE DECAY

The photon-pair source in this work is based on the $\chi^{(3)}$ nonlinear susceptibility of ^{87}Rb. A similar scheme was initially demonstrated with a different choice of transitions and, consequently, wavelengths [24]. The relevant electronic structure is shown in Fig. 1(a). Two pump beams of wavelength 780 nm (pump 1) and 776 nm (pump 2) excite the atoms from $5S_{1/2}$, $F = 2$ to $5D_{3/2}$, $F = 3$ via a two-photon transition. The 780 nm pump is red detuned by Δ from the intermediate
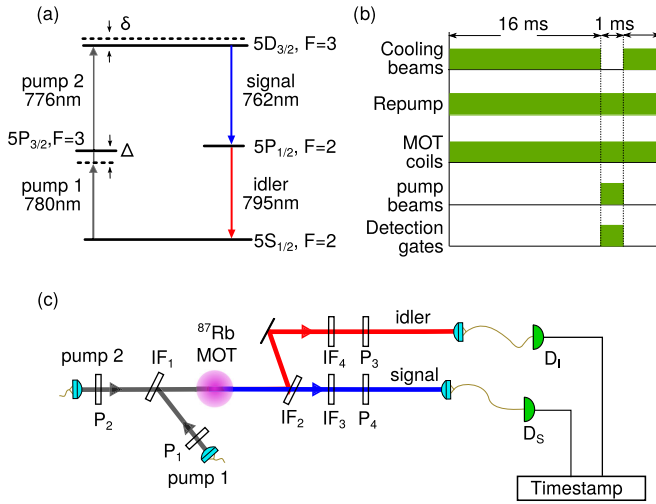
FIG. 1. (a) Cascade-level scheme used for parametric conversion in atoms. (b) Timing sequence of the experiment. (c) Schematic of the experimental setup, with P1, P2, P3, and P4: polarization filters; IF$_1$, IF$_2$, IF$_3$, and IF$_4$: interference filters; D$_I$, D$_S$: avalanche photodetectors.

level $5P_{3/2}$, $F = 3$ to reduce the rate of incoherent scattering, with Δ between 30 and 60 MHz. The two-photon detuning δ is one of the parameters we study in this work.

The subsequent decay from the excited level $5D_{3/2}$, $F = 3$ to the ground state $5S_{1/2}$, $F = 2$ via $5P_{1/2}$, $F = 2$ generates a pair of photons with wavelengths centered around 795 nm (signal) and 762 nm (idler). We reject light originating from other scattering processes using narrow-band interference filters. The geometry of the pump and collection modes is chosen to satisfy the phase-matching condition. Energy conservation ensures time correlation of the generated photons, while the time ordering imposed by the cascade decay results in a strongly asymmetrical time envelope of the biphoton. This coherent process is accompanied by incoherent scattering. Both processes generate light at the same wavelengths, making it impossible to distinguish them by spectral filtering. Similar to simple two-level systems [25,26], coherent and incoherent scattering have different dependencies on a number of experimental parameters.

To understand the difference in behavior, we consider a long-established model of a strongly driven three-level atom [27,28]. This simple model correctly describes some of the features of our photon-pair source. In this model, the atomic state is described by the 3×3 density matrix ρ, where state 1 corresponds to the ground state, state 3 to the most excited state, and state 2 to the intermediate state in the cascade decay. The total scattering rate, that includes both coherent and incoherent events, is proportional to the population in state 3,

$$r_{tot} \propto \langle \rho_{33} \rangle, \tag{1}$$

while the signal we are interested in is proportional to the coherence between states 1 and 3,

$$r_{coh} \propto |\langle \rho_{31} \rangle|^2. \tag{2}$$

Following [27], we derive an analytical steady-state solution of the master equation as function of the pump intensities (through

the corresponding Rabi frequencies Ω_1 and Ω_2) and detunings (Δ and δ) [1].

In order to compare Eq. (1) and Eq. (2) to our experimental results, we need to take into account the linewidths of the pump lasers. A rigorous approach would require the inclusion of the laser linewidth in the master equation [29]. For large Rabi frequencies, as in our case, the spectral broadening associated with the laser power dominates. We can therefore approximate the combination of the two pump lasers Lorentzian profiles of width ≈ 1 MHz into a single noise spectrum with Gaussian profile $G(\delta)$ of width ≈ 2 MHz. We obtain a fitting function for our results by convolving Eqs. (1) and (2) with the combined linewidth of the pump lasers,

$$r_{single} \propto r_{tot}(\Omega_1, \Omega_2, \Delta, \delta) * G(\delta) \tag{3}$$

and

$$r_{pairs} \propto r_{coh}(\Omega_1, \Omega_2, \Delta, \delta) * G(\delta). \tag{4}$$

The heralding efficiency for photons (in a scenario where one photon is used as a herald for the presence of the other) is the ratio of these rates:

$$\eta = \frac{r_{pairs}}{r_{single}} = \frac{r_{coh}(\Omega_1, \Omega_2, \Delta, \delta) * G(\delta)}{r_{tot}(\Omega_1, \Omega_2, \Delta, \delta) * G(\delta)}. \tag{5}$$

This model does not take into account the Zeeman manifold of the energy levels, nor the collective interaction within the atomic ensemble. We already presented a model and experimental evidence of the effects of polarization choice for pumps and collection modes previously [21]. In the rest of this article, the polarization of the pump beams and collection modes is chosen to maximize the effective nonlinearity and, consequently, maximize the generation rates. To understand the effect of collective interaction in a cascaded decay process we compare our results with the model proposed in [30] in Sec. V.

III. EXPERIMENTAL SETUP

The experimental setup is shown in Fig. 1(c). The nonlinear medium is an ensemble of ^{87}Rb atoms in a vacuum chamber (pressure 1×10^{-9} mbar), trapped and cooled with a magneto-optical trap (MOT) formed by a pair of circular coils connected in an anti-Helmholtz configuration generating a magnetic-field gradient of 24.8 G/cm in the radial direction and 49.6 G/cm in the axial direction and six laser beams red detuned by 24 MHz from the cycling transition $5S_{1/2}$, $F = 2 \rightarrow 5P_{3/2}$, $F = 3$, with a diameter of 15 mm and an optical power of 45 mW per beam. No compensation was used for any residual magnetic field. An additional laser tuned to the $5S_{1/2}$, $F = 1 \rightarrow 5P_{3/2}$, $F = 2$ transition optically pumps the atoms back into the $5S_{1/2}$, $F = 2$ level.

The low temperature of the ensemble (estimated from similar experimental setups [31] to be equal to or smaller than the Doppler temperature of ^{87}Rb of 146 μK) ensures a negligible Doppler broadening of the atomic transition line,

resulting in a reduction of the bandwidth of the generated photons by an order of magnitude compared to the hot vapor sources [32,33].

In its initial implementation [18], the source was non-collinear, i.e., pump and collection modes do not lie on the same axis. This approach was chosen to minimize the collection of any pump light into the parametric fluorescence modes. In subsequent experiments, including this work, we instead chose a collinear configuration. This geometry simplifies the alignment and allows for a more efficient coupling of the generated photons into single mode fibers. We combine the pump beams (780 nm and 776 nm) using a narrow-band interference filter (IF$_1$) as a dichroic mirror. Similarly, we separate the signal (762 nm) and idler (795 nm) modes using another interference filter (IF$_2$). The pump and collection modes are focused in the cloud. Both pumps have a beam waist of $\approx$0.45 mm, while the collection modes are $\approx$0.4 mm and $\approx$0.5 mm for signal and idler, respectively. Leaking of pump light into the collection modes is reduced by an additional interference filter in each collection mode (IF$_3$, IF$_4$). All interference filters used in the setup have a full width at half maximum bandwidth of 3 nm and a peak transmission 96% at 780 nm. We tune their transmission frequencies by adjusting the angles of incidence. Polarizers P$_1$ and P$_2$ fix the polarization of the fluorescence before collecting it into single mode fibers with aspheric lenses. Single photons are detected using avalanche photodiodes (APD) with quantum efficiency of $\approx$50%.

Figure 1(b) shows the timing sequence used in the experiment: 16 ms of cooling of the atomic vapors, followed by a 1 ms time window, during which the cooling beams are off and pump 1 and pump 2 shine on the cloud. We use external-cavity laser diodes (ECDL) with bandwidths in the order of 1 MHz to generate the pumps, and control their power and detuning using acousto-optic modulators (AOM).

IV. DETECTION OF PHOTON PAIRS

We characterize the properties of the source from the statistics and correlation of detection times for events in the signal and idler modes. All detection events are time stamped with a resolution of 125 ps. Figure 2 shows a typical coincidence histogram $G^{(2)}$, i.e., the coincidence counts as a function of the delay between detection times Δt. The correlation function shows an asymmetric shape: a fast rise followed by a long exponential decay. The rise time is limited by the jitter time of the APDs (typical value $\approx$800 ps), while the decay is a function of the coherence time. In a previous work [18] we showed that the bandwidth is inversely proportional to the decay time constant τ. We measure τ by fitting the histogram $G^{(2)}$ with the function

$$G^{(2)}_{\text{fit}}(\Delta t) = G_{\text{acc}} + G_0\, e^{-\Delta t/\tau}\,\Theta(\Delta t), \qquad (6)$$

where G_{acc} is the rate of accidental coincidences, Θ is the Heaviside step function, and G_0 an amplitude. The rate of accidental coincidences G_{acc} is fixed by considering the average of $G^{(2)}$ for times Δt much larger than the coherence time, leaving as free parameters only G_0 and τ. This can be used to estimate the second-order cross-correlation function $g^{(2)}$ from Eq. (6):

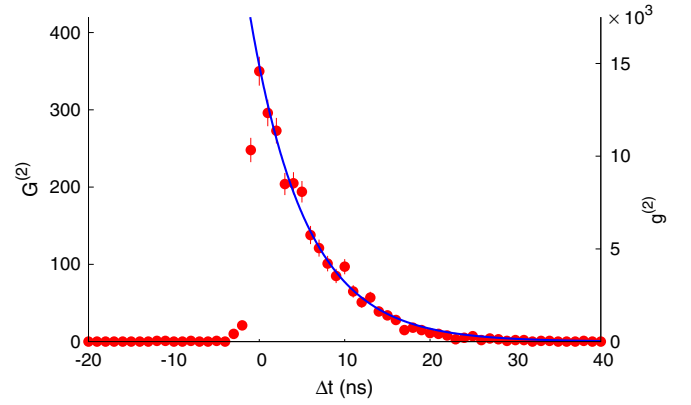$$g^{(2)}(\Delta t) = G^{(2)}_{\text{fit}}(\Delta t)/G_{\text{acc}}. \qquad (7)$$

FIG. 2. Histogram of coincidence events $G^{(2)}(\Delta t)$ (left vertical axis) and the normalized second-order correlation $g^{(2)}(\Delta t)$ (right vertical axis) as a function of the time difference between the detection of signal and idler photons for a total integration time of 42 s. Pump powers: $P_{780} = 450\ \mu$W and $P_{776} = 3$ mW; detunings: $\Delta = -60$ MHz and $\delta = 12$ MHz. The solid line is a fit to the model described by Eq. (6), giving a value of $\tau = 6.52 \pm 0.04$ ns.

To characterize the source, we consider the rate of single event detection in the signal (r_s) and idler (r_i) modes, together with the rate of coincidence detection (r_p) as the signature of photon pairs. All reported rates are instantaneous rates in the parametric conversion part of the cooling or photon generation cycle.

The total pair detection rate r_p of the source is obtained by integrating $G^{(2)}(\Delta t)$ over a coincidence time window $0 < \Delta t < \Delta t_c$. We choose $\Delta t_c = 30$ ns to ensure the collection of a large fraction of events also for the largest coherence times τ observed.

Another parameter we extract from the measured $G^{(2)}(\Delta t)$ is heralding efficiency. Due to the intrinsic asymmetry of the process we define two heralding efficiencies from the same measurement, one for the signal,

$$\eta_{\text{S}} = r_p/(r_{\text{S}} - d_{\text{S}}), \qquad (8)$$

and one for the idler,

$$\eta_{\text{I}} = r_p/(r_{\text{I}} - d_{\text{I}}), \qquad (9)$$

where $d_{\text{S}} = 508$ s^{-1} and $d_{\text{I}} = 165$ s^{-1} are the dark count rates on the signal and idler detectors.

V. EFFECT OF THE NUMBER OF ATOMS

One of the parameters of interest is the number of atoms N participating in the four-wave mixing process. We control it by varying the optical power of the repump light during the cooling phase, thus changing the atomic density without altering the geometry of the optical trap.

We estimate N by measuring the optical density (OD) D of the atomic ensemble for light resonant with the $5S_{1/2}, F = 2 \rightarrow 5P_{3/2}, F = 3$ transition. To obtain a reliable measure of the OD, we turn off pump 2 and set pump 1 to 10 μW, more than 40 times lower than the saturation intensity of the transition of interest. We record the transmission of pump 1 through the vacuum cell for a range of values of Δ wide enough to capture the entire absorption feature, and normalize it to the
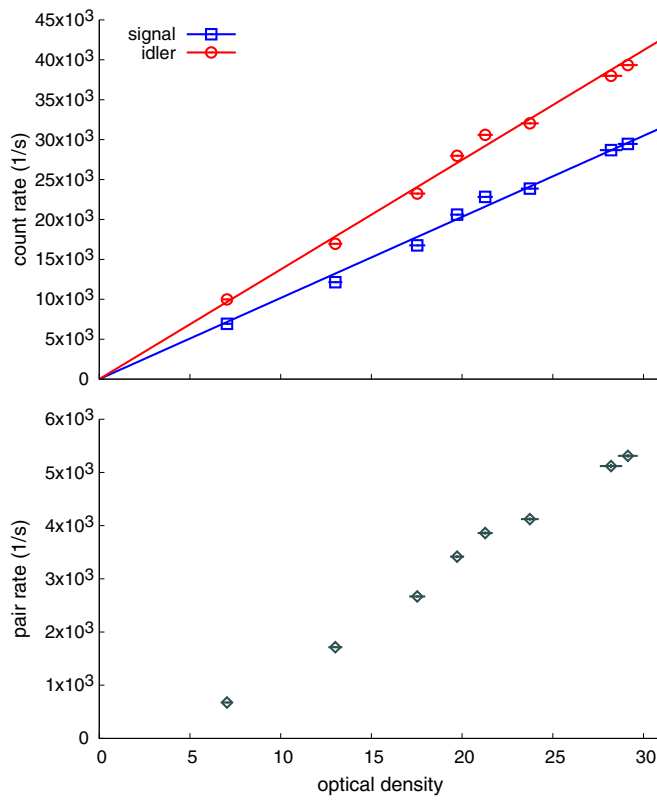
FIG. 3. Rate of single counts in the signal and idler modes (top) and rate of coincidence counts (bottom) as a function of the optical density (OD) of the atomic cloud. The solid lines are fits for $r_{s,i} = a_{s,i} D$, with $a_{s,i}$ the only free parameter. Other parameters: $P_{776} = 15$ mW, $P_{780} = 300$ μW, $\Delta = -60$ MHz, and $\delta = 12$ MHz.

transmission observed without the atomic cloud. We fit the measurement results with the expected transmission spectrum

$$T(\Delta) = \exp\left(-D\frac{\gamma^2}{\Delta^2 + \gamma^2}\right),\qquad(10)$$

with $\gamma = 6.067$ MHz and OD as the only free parameter. From the size of the probe beam $w_0 \approx 450$ μm, we estimate N. We observed a minimum of $N \approx 1.5 \times 10^7$, corresponding to an OD ≈ 7, and a maximum of $N \approx 6.3 \times 10^7$, OD ≈ 29. We expect the effective number of atoms participating in the FWM process to decrease during the measurement due to the heating caused by the intense pumps.

Single detection rates for the signal (r_s) and idler (r_i) modes increase linearly with the number of atoms involved in the process, as expected for incoherent processes (see Fig. 3). The increase of pair rate r_p with N, however, appears to be faster than linear.

Further, the decay or coherence time τ decreases in our experiments as OD increases (see Fig. 4). The measured coherence time is always shorter than the natural lifetime $\tau_0 = 27$ ns of the intermediate state expected for the spontaneous decay in free space of this transition to the ground state of ^{87}Rb. This is a signature of collective effects in the cold atom cloud [18,34]. The solid line is a fit to the theoretical model
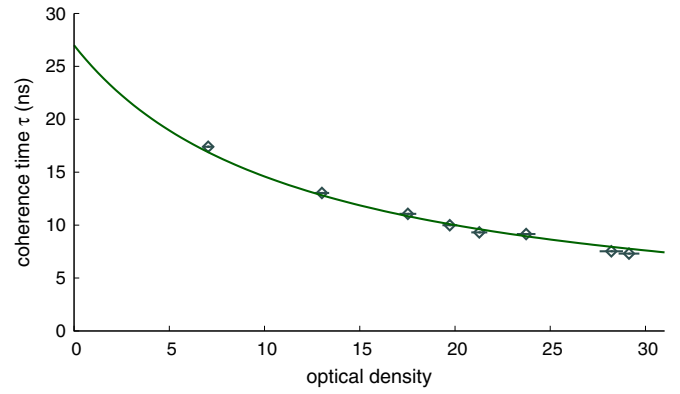

FIG. 4. Coherence time of the photon pair as a function of the optical density (OD) of the atomic cloud. The solid line is obtained by fitting Eq. (11), obtaining $\mu = 0.0827 \pm 0.002$. Other parameters: $P_{776} = 15$ mW, $P_{780} = 300$ μW, $\Delta = -60$ MHz, and $\delta = 12$ MHz.

proposed in [30]:

$$\tau = \frac{\tau_0}{1 + \mu D},\qquad(11)$$

where the free parameter μ is a geometrical constant depending on the shape of the atomic ensemble.

We do not have a complete explanation for the nonlinear increase of the pair rate with the optical density, but some insight can be gained from the heralding efficiencies shown in Fig. 5. Both heralding efficiencies η_s and η_i exhibit a saturation behavior that is described by the relation

$$\eta_j = \eta_{0j}\left[1 - \exp\left(-\frac{D}{D_{0j}}\right)\right] \quad \text{with } j = s, i,\qquad(12)$$

where η_{0j} and D_{0j} are free parameters. This heuristic expression suggests that (a) a higher optical density of the atomic cloud leads to an increase of the pair rate at the expense of a larger photon bandwidth and (b) for large enough OD there is no improvement of heralding efficiency. These considerations are particularly relevant considering the recent development
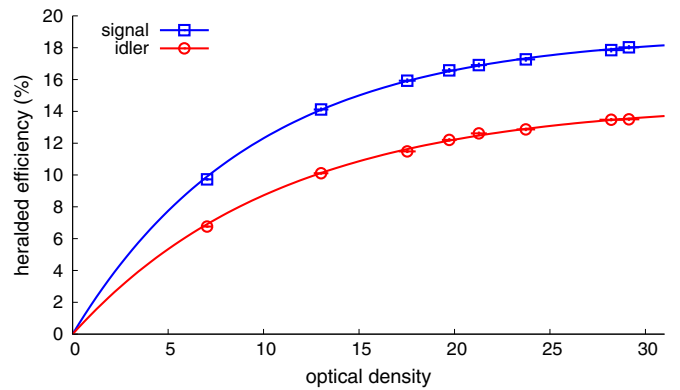

FIG. 5. Heralding efficiency for signal and idler modes as a function of the optical density. The solid lines are fits of Eq. (12) with $\eta_{0s} = 0.190 \pm 0.001$ and $D_{0s} = 9.7 \pm 0.1$, and $\eta_{0i} = 0.150 \pm 0.001$ and $D_{0i} = 11.3 \pm 0.2$. Other parameters: $P_{776} = 15$ mW, $P_{780} = 300$ μW, $\Delta = -60$ MHz, and $\delta = 12$ MHz.
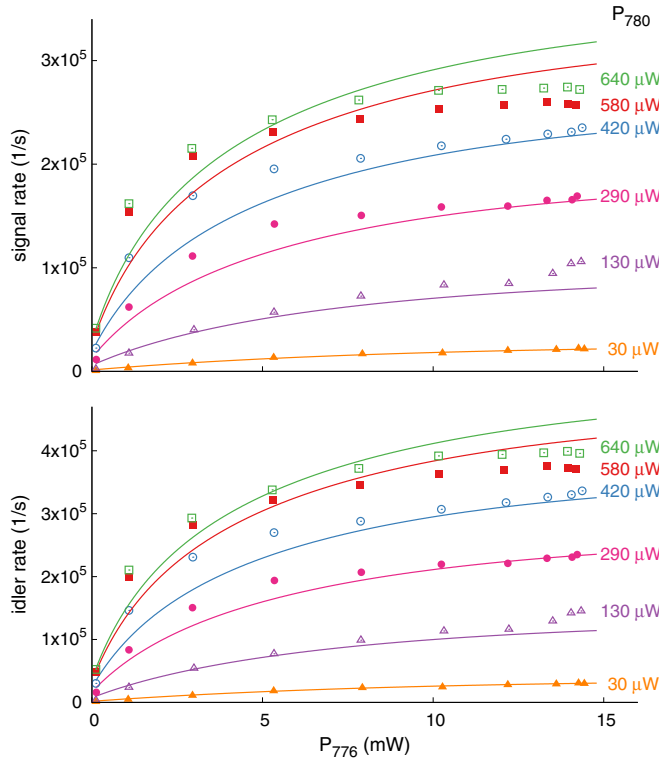
FIG. 6. Single rates for the signal (top) and idler (bottom) as a function of pump power at 776 nm (P_{776}) for different pump powers at 780 nm. The vertical error bar on each point is smaller than the size of the data points. Other parameters: $D = 29$, $\Delta = -60$ MHz, and $\delta = 3$ MHz. The solid lines are numerical fits with Eq. (3).

FIG. 7. Pair rates as function of pump power at 776 nm (P_{776}) for different pump powers at 780 nm. The vertical error bar on each point is smaller than the size of the data points. The solid lines are calculated from the theory. Other parameters: $D = 29$, $\Delta = -60$ MHz, and $\delta = 3$ MHz. The solid lines are numerical fits with Eq. (4).

of cold atomic systems with optical densities in excess of 500 [35].

By fitting Eq. (12) to the experimental data, we obtain $\eta_{0s} = 0.190 \pm 0.001$ and $D_{0s} = 9.7 \pm 0.1$ for the signal and $\eta_{0i} = 0.150 \pm 0.001$ and $D_{0i} = 11.3 \pm 0.2$ for the idler.

VI. RATES AND HERALDING EFFICIENCIES

Brightness, a common parameter to characterize a photon-pair source, is defined as the experimentally accessible rate of photon pairs emitted into the desired modes per mW of pump power. In our source, saturation effects of the atomic transitions involved give rise to a nonlinear correlation between pump power and rates. In Figs. 6 and 7, the instantaneous single rates, r_s and r_i, and pair rates r_p as a function of power in both pump transitions are shown.

For a fixed two-photon detuning δ, all rates exhibit a saturation behavior. This suggests that an increase of the pump powers will increase the observed pair rate only to some extent, and an increased number of atoms of the ensemble might be a better option. However, as discussed in the previous section, this comes at the expense of a larger bandwidth. We also note that, while the model introduced in Sec. II qualitatively explains the saturation behavior with the pump powers, it does not capture well the experimental observation for high powers. This is probably due to the optical pumping caused by the intense pump beams, which is not part of the relatively simple model.
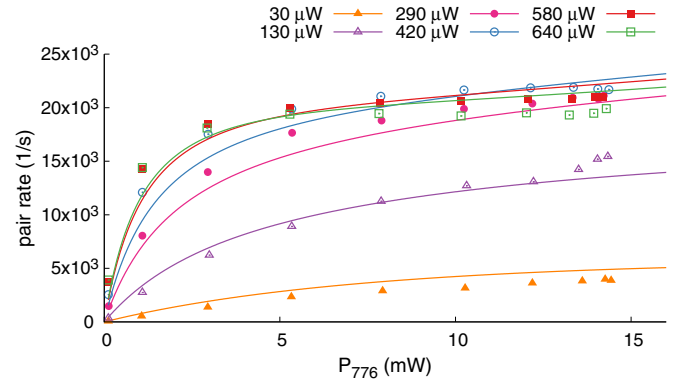
The dependency of heralding efficiencies on both pump powers is shown in Fig. 8, both for our experimental observations and the model predictions.

The intuition of a higher heralding efficiency at low pump powers due to a smaller contribution from incoherent processes
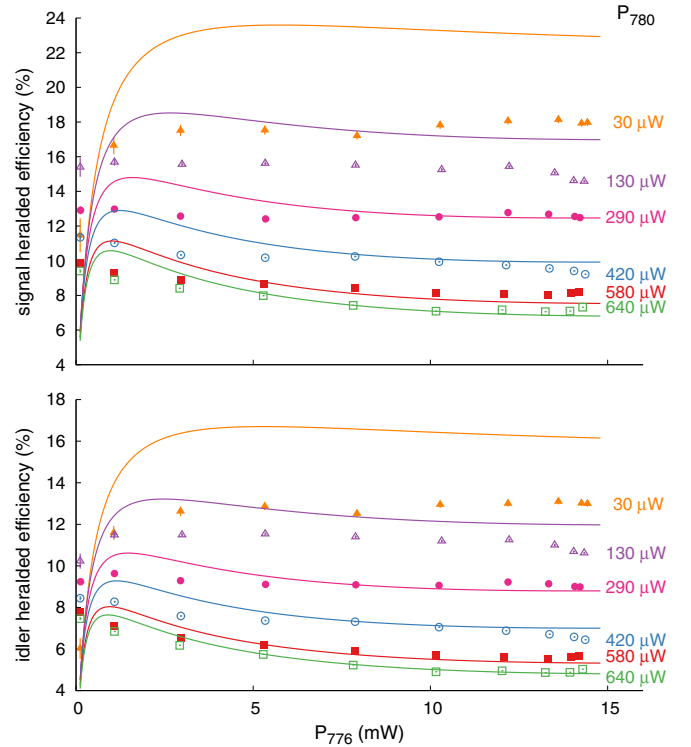

FIG. 8. Heralding efficiency as function of P_{776} for the signal (top) and idler (bottom) for different P_{780}. The vertical error bar on each point is smaller than the size of the data points. Other parameters: $D = 29$, $\Delta = -60$ MHz, and $\delta = 3$ MHz. The solid lines are a numerical fit with Eq. (5). The model fails to describe the experimental behavior for low pump powers. As discussed in the main text, in this region the power broadening is comparable with the pump laser linewidths, a regime beside the model assumptions.
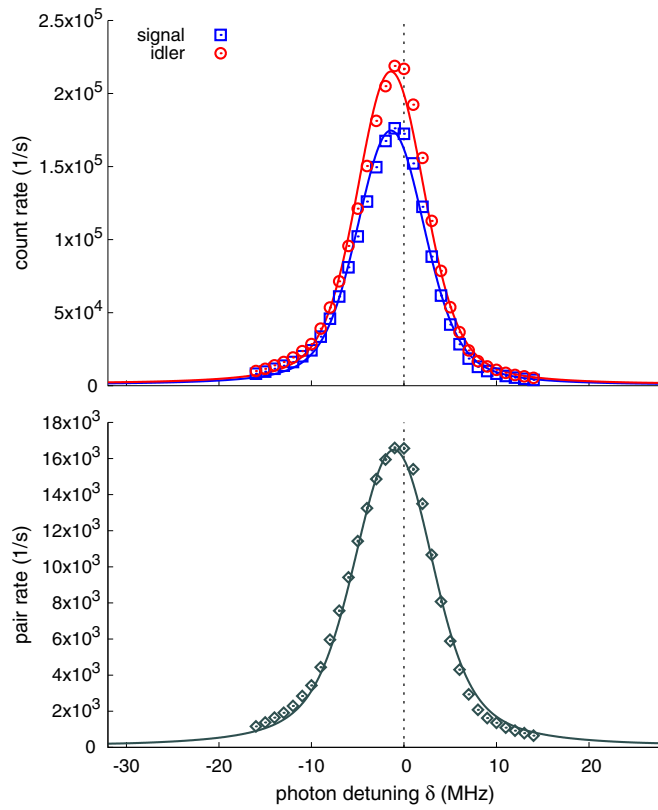
FIG. 9. (Top) Single count rates as a function of the detuning from the two-photon resonance δ. The solid lines are numerical fits of Eq. (3). (Bottom) Pair rate (r_p) as a function of δ. The solid line is a numerical fit of Eq. (4). Other parameters: $P_{776} = 15$ mW, $P_{780} = 450$ μW, $\Delta = -60$ MHz, and $D = 29$. The dotted line indicates $\delta = 0$.

[314] is both found in the experiment and predicted by the model,
[315] but the model does not match the observations at low powers
[316] very well. A possible explanation is in one of the assumptions
[317] of our model. For low pump powers, the broadening due
[318] to Rabi frequencies of the pumps is comparable with the
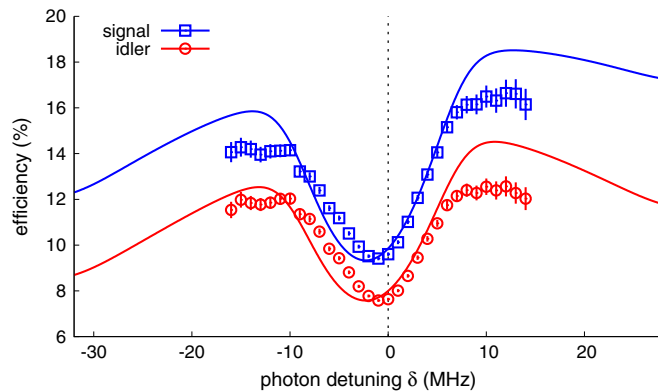[319] pump laser linewidths, requiring then a different approach than

FIG. 10. Efficiency of the source as a function of the detuning from the two-photon resonance δ. Other parameters: $P_{776} = 15$ mW, $P_{780} = 450$ μW, $\Delta = -60$ MHz, and $D = 29$. The solid lines are fits with Eq. (5); the dotted line indicates $\delta = 0$.
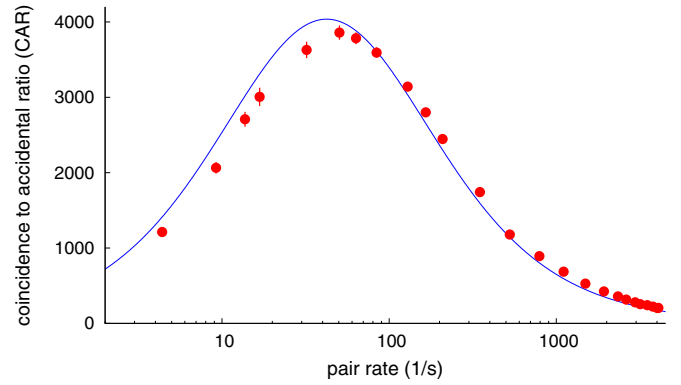

FIG. 11. Coincidence to accidental ratio (CAR) as a function of pair rates r_p. The solid line is obtained from Eq. (14) with $\eta_S = 17.3\%$, $\eta_I = 12.4\%$, $d_S = 165$ s^{-1}, $d_I = 508$ s^{-1}, and $\Delta t = 30$ ns.

convolution with a combined noise spectrum. However, our [320] simple model ignores all geometrical aspects in the process, [321] and therefore does not capture any spatial variation of the [322] atomic density profile of the cloud, the intensity profile of the [323] pump beams, or their respective overlap. [324]

Despite the limitations of the model, the observed power [325] dependency of pair rates and heralding efficiency shown in [326] Figs. 7 and 8 suggest a strategy for optimizing the source [327] brightness: a low power P_{780} on the transition depopulating the [328] ground state should ensure a high heralding efficiency, while a [329] high power P_{776} on the transition populating the state 3 should [330] increase the brightness. An obvious experimental limitation to [331] this strategy for rubidium is the available P_{776}. [332]

Apart from the optical power in the pump beams, other [333] easily available experimental parameters in the four-wave [334] mixing process are the pump detunings. Both single and pair [335] rates have a strong dependence on the two-photon detuning δ [336] from the ground state in the upper excited state, and have a [337] maximum at $\delta \approx 0$, as expected for a scattering process (see [338] Fig. 9). The two-step nature of the excitation process leads [339] to asymmetries in the peaks, which is also predicted by the [340] simple model of Eqs. (3) and (4). To allow for a fair comparison [341] between the model prediction and the experimental data, we [342] have to take into account the linewidth of the pump lasers ($\approx$1 [343] MHz each). We therefore convolve the theoretical predictions [344]
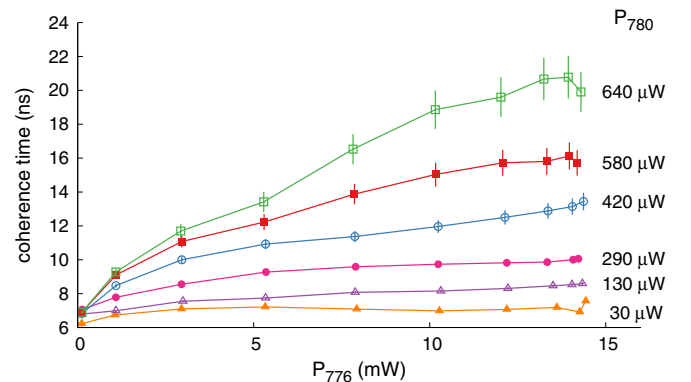

FIG. 12. Coherence time as function of pump powers. Other parameters: $D = 29$, $\Delta = -60$ MHz, and $\delta = 3$ MHz.
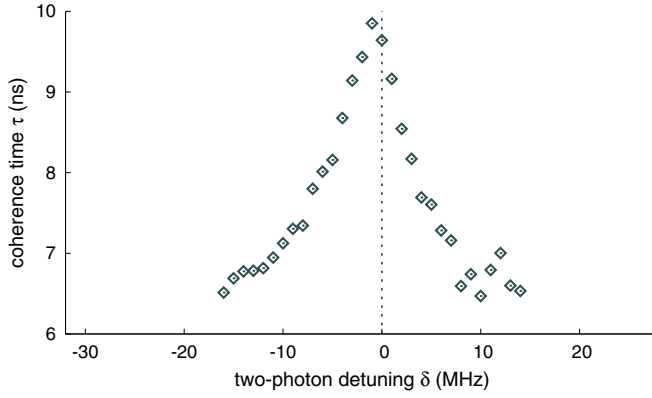
FIG. 13. Coherence time as function of detuning. Other parameters: $P_{776} = 15$ mW, $P_{780} = 450$ μW, $\Delta = -60$ MHz, and $D = 29$. The dotted line indicates $\delta = 0$.

in Eqs. (3) and (4) with a Gaussian distribution modeling our laser noise. The resulting spectral profiles in the two-photon detuning of pair and single rates then match very well the behavior observed in our experiment.

Contrary to the single and pair rates, both heralding efficiencies show an asymmetric dip around $\delta \approx 0$ (see Fig. 10) in our experiment, which is well captured by the model via Eq. (5).

This dip can be understood by taking into account that the observed single rate is the combination of FWM, a coherent process, and incoherent scattering, with the latter growing faster as δ approaches zero. When choosing the operation parameter of a photon-pair source for subsequent use, the two-photon detuning can therefore be optimized for a compromise between pair rate and heralding efficiency.
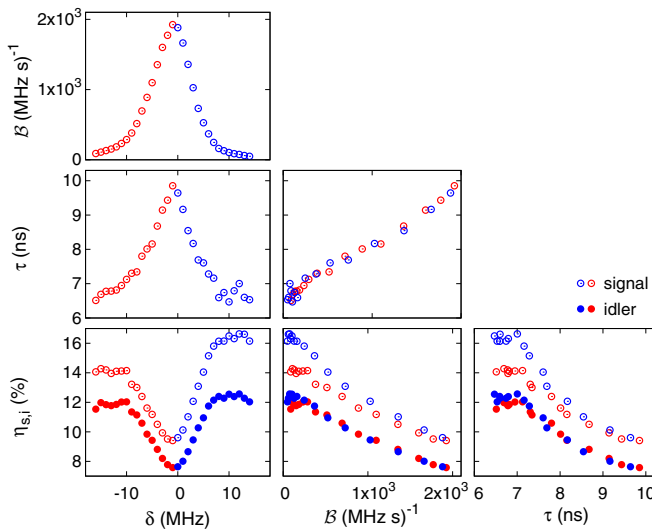

FIG. 14. Summary of the effect of two-photon detuning δ on heralding efficiencies $\eta_{s,i}$, coherence time τ, and spectral brightness $\mathcal{B}$. Other parameters: $P_{776} = 15$ mW, $P_{780} = 450$ μW, $\Delta = -60$ MHz, and $D = 29$.

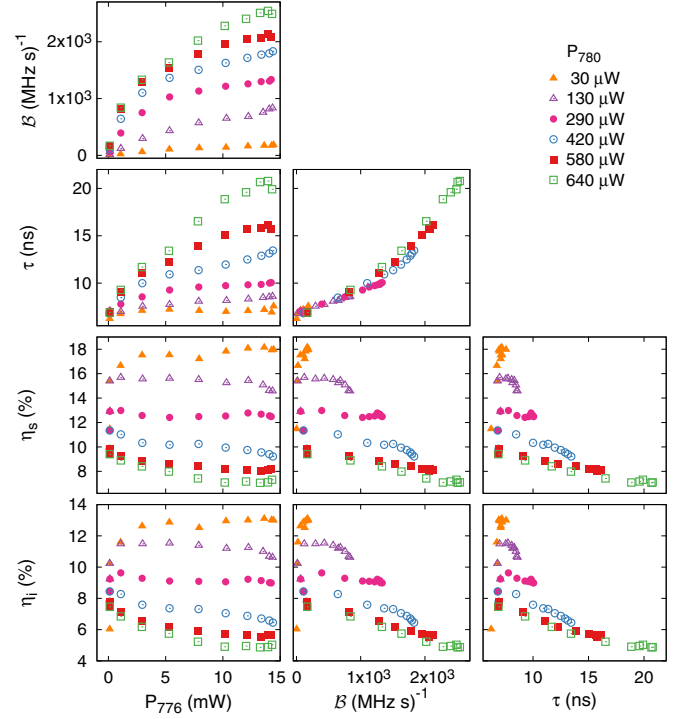FIG. 15. Summary of the effect of pump powers P_1 and P_1 on heralding efficiencies $\eta_{s,i}$, coherence time τ, and spectral brightness $\mathcal{B}$. Other parameters: $D = 29$, $\Delta = -60$ MHz, and $\delta = 3$ MHz.

VII. COINCIDENCE TO ACCIDENTAL RATIO (CAR)

Another relevant parameter for characterizing the usefulness of a source of photon pairs is the coincidence to accidental ratio (CAR) [36,37],

$$C = \frac{R_p}{r_a} = \frac{r_I\, r_S\, \Delta t + r_p}{r_I\, r_S\, \Delta t}, \tag{13}$$

where the accidental rate r_a captures noise photons that degrade the correlation characteristics of the photon-pair source. The connection between the CAR and pair rate r_p is shown in Fig. 11. In this parametric plot, we vary the pump power P_{776}. Over a wide range of pair rates, the CAR increases when P_{776} is reduced because $r_a \overset{\propto}{\sim} r_p^2$. For the experimental parameters shown in this measurement, the CAR peaks at ≈ 3800, at a relatively low pair rate of $r_p = 50$ s^{-1}. With a further reduction in pump power (and therefore in r_p), the CAR drops to 1, as background noise and detector's dark counts (r_a) dominate in Eq. (13).

To model the experimentally observed CAR, we modify the expression in Eq. (13) by separating the single rates for signal and idler into a contribution from pairs, corrected by the respective heralding efficiencies, and dark or background contributions for signal and idler. Signal and idler heralding efficiencies vary very little over a wide range of pump powers P_{776}, so we fix them to a single value. The resulting expression for the CAR,

$$C = \frac{\left(\frac{r_p}{\eta_S} + d_S\right)\left(\frac{r_p}{\eta_I} + d_I\right)\Delta t + r_p}{\left(\frac{r_p}{\eta_S} + d_S\right)\left(\frac{r_p}{\eta_I} + d_I\right)\Delta t}, \tag{14}$$
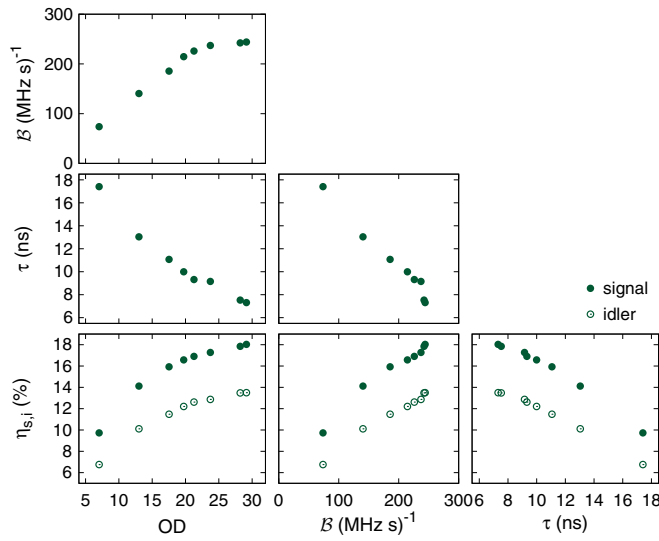
FIG. 16. Summary of the effect of optical density OD on heralding efficiencies $\eta_{s,i}$, coherence time τ, and spectral brightness $\mathcal{B}$. Other parameters: $P_{776} = 15$ mW, $P_{780} = 300$ μW, $\Delta = -60$ MHz, and $\delta = 12$ MHz.

reproduces very well the observed behavior in the experiment, suggesting that the relation between CAR and pair rates is fairly well understood.

VIII. COHERENCE TIME OF THE GENERATED PAIRS

An important property of photon-pair sources based on nonlinearities is the small bandwidth of the emerging photons corresponding to a long coherence time. The dependency of the coherence time, measured by fitting photon-pair timing histograms to Eq. (6), on pump power and two-photon detuning, is shown in Figs. 12 and 13. The coherence time increases with both pump powers, and also shows a maximum with respect to the two-photon detuning slightly below the two-photon resonance, similar to the pair rates.

The simple three-level model in Sec. II does not address the coherence time of the emerging photons. Even a more complex model that includes the collective effects associated with the number of atoms [30] predicts only a dependency of the coherence time on the number of atoms involved in the four-wave mixing process (superradiance), but not on the pump power and two-photon detuning. A possible reason for the observed dependency is a decay from the excited state $5P_{1/2}$, $F = 3$ to $5S_{1/2}$, $F = 1$, a ground state that does not participate in the coherent four-wave mixing we are interested in, effectively depleting the number of atoms interacting with the pump beams. This depletion increases with pump intensities, and decreases with detuning, and is not completely neutralized by the repump beam, resulting in a change of the number of atoms in the participating ground state, which would then affect the coherence time according to the more complex conversion model [30].

To arrive at long coherence times, one therefore would need to optimize the repumping process during the parametric conversion cycle in our experiment to maintain the atomic population in the ground state.

IX. GUIDELINES FOR CHOICE OF PARAMETERS

Following our characterization of this photon-pair source, it is useful to introduce some guidelines for the choice of operational parameters. We summarize the effects of the different experimental knobs in Figs. 14, 15, and 16. We included the heralding efficiency, coherence times, and spectral brightness $\mathcal{B} = 2\pi \tau r_p$. Some trends are common: heralding efficiencies and coherence time appear to be inversely correlated, independent of the parameters we are varying. In experiments where the generated photon pairs interact with atomic systems it is often important to maximize the spectral brightness. In this case, it is necessary to maximize the optical density, set the two-photon detuning a few MHz red off resonance, and maximize both pump powers. If the target is to maximize the heralding efficiency, it is convenient to increase the two-photon detuning, and reduce power P_{780} until a suitable compromise between heralding efficiency and brightness is reached.

X. CONCLUSION

We presented an experimental study of the effect of two-photon detuning, pump intensity, and number of atoms on the generation rates and bandwidth of photon pairs from four-wave mixing in a cold ensemble of rubidium atoms. The study is useful to understand how to set the different parameters to better exploit the source characteristics, in particular when combined with other, generally very demanding, atomic systems [22,23].

The effect of pump powers and two-photon detuning on pair rates and efficiencies is compatible with the theoretical model presented by Whitley and Stroud [27]. An increase in pump power corresponds to an increase of pair and singles rates until a saturation level, with heralding efficiency determined mostly by the ground-state resonant pump. We can also explain the connection between the coincidence to accidental ratio (CAR) and the generated pair rates. All rates increase with a reduction of the two-photon detuning at the expense of heralding efficiency. This is well captured by the model, and can be intuitively explained as the result of competition between coherent and incoherent scattering processes excited by the same optical pumps.

One of the attractive aspects of cold-atom based photon-pair sources is their frequency characteristics: the generated pairs are usually resonant or close to resonant with their bandwidth of the same order of magnitude as atomic transitions. In our source the central wavelengths are fixed; the bandwidth instead is a function of the experimental parameters, in particular of the number of atoms. The dipole-dipole interaction between atoms gives rise to superradiance [38], as evidenced by the reduction of coherence time as the number of atoms increases [30]. But the total number of atoms is also a function of duration, intensity, and detuning of the pump beams because of optical pumping. The dynamics of the combined effect of collective interaction between atoms and optical pumping increases the complexity of the phenomenon, and we currently do not have a model that fully explains our result. Nonetheless, the experimental measurements are a useful guide to choose the number of atoms, together with the other parameters, that optimizes the specific properties desired from the source: rate, heralding efficiency, or bandwidth.

APPENDIX: EXPLICIT FORM OF EQ. (1) and EQ. (2)

In the following expressions, Γ_1 and Γ_1 are the linewidths of the transitions addressed by pumps 1 and 2, respectively:

$$\langle \rho_{33} \rangle = \frac{\Omega_1^2 \Omega_2^2 \left(\Gamma_1 \Gamma_2 ((\delta - \Delta)^2 + (\Gamma_1 + \Gamma_2)^2) + \Gamma_1 \Omega_1^2 (\Gamma_1 + \Gamma_2) + \Omega_2^2 (\Gamma_1 + \Gamma_2)^2 \right)}{K}, \tag{A1}$$

$$\begin{aligned}
|\langle \rho_{31} \rangle|^2 = \left| \frac{\Omega_1 \Omega_2}{K} \right|^2 \Big| & \delta^3 \Gamma_1 \Gamma_2 (\Delta - i\Gamma_1) - \delta^2 \Gamma_1 \Gamma_2 \big((\Delta - i\Gamma_1)(2\Delta + i\Gamma_2) + \Omega_1^2 + \Omega_2^2 \big) + \delta \Gamma_1 \big(\Gamma_2 (\Delta - i\Gamma_1)(\Delta^2 + 2i\Delta\Gamma_2 \\
& + (\Gamma_1 + \Gamma_2)^2) + \Omega_2^2 (\Delta(\Gamma_1 + 3\Gamma_2) - i\Gamma_1(\Gamma_1 + \Gamma_2)) + 2i\Gamma_2 \Omega_1^2 (\Gamma_1 + \Gamma_2) \big) - i\Delta^3 \Gamma_1 \Gamma_2^2 - \Delta^2 \Gamma_1 \Gamma_2 \big(\Gamma_1 \Gamma_2 - \Omega_1^2 + \Omega_2^2 \big) \\
& - i\Delta\Gamma_1 \Gamma_2 (\Gamma_1 + \Gamma_2) \big(\Gamma_2(\Gamma_1 + \Gamma_2) + 2\Omega_1^2 + \Omega_2^2 \big) - \big(\Gamma_1 \Gamma_2 (\Gamma_1 + \Gamma_2) + \Gamma_1 \Omega_2^2 - \Gamma_2 \Omega_1^2 \big) \\
& \times \big(\Gamma_1 \big(\Gamma_2(\Gamma_1 + \Gamma_2) + \Omega_1^2 \big) + \Omega_2^2 (\Gamma_1 + \Gamma_2) \big) \Big|^2,
\end{aligned} \tag{A2}$$

with

$$\begin{aligned}
K = {} & \delta^4 \Gamma_1 \Gamma_2 \big(\Delta^2 + \Gamma_1^2 + 2\Omega_1^2 \big) - 2\delta^3 \Delta \Gamma_1 \Gamma_2 \big(\Delta^2 + \Gamma_1^2 + 2\Omega_1^2 + \Omega_2^2 \big) + \delta^2 \big(\Omega_2^2 (\Delta^2 \Gamma_1 (\Gamma_1 + 5\Gamma_2) + \Gamma_1^2 (\Gamma_1^2 + \Gamma_1 \Gamma_2 + 2\Gamma_2^2) \\
& + 2\Omega_1^2 (\Gamma_1 + \Gamma_2)^2) + \Gamma_1 \Gamma_2 \big(\Delta^2 + \Gamma_1^2 + 2\Omega_1^2 \big) \big(\Delta^2 + \Gamma_1^2 + 2\Gamma_1 \Gamma_2 + 2\Gamma_2^2 - 2\Omega_1^2 \big) + \Gamma_1 \Gamma_2 \Omega_2^4 \big) \\
& + 2\delta\Delta \big(-\Gamma_2 \Omega_2^2 (\Gamma_1(\Delta^2 + \Gamma_1^2 + 4\Gamma_1 \Gamma_2 + \Gamma_2^2) + \Gamma_2 \Omega_1^2) + \Gamma_1 \Gamma_2 (\Omega_1^2 - \Gamma_2^2)(\Delta^2 + \Gamma_1^2 + 2\Omega_1^2) - \Gamma_1 \Omega_2^4 (\Gamma_1 + 2\Gamma_2) \big) \\
& + \Delta^4 \Gamma_1 \Gamma_2^3 + \Delta^2 \Gamma_2 \big(\Gamma_1 \big(\Gamma_2^2 (2\Gamma_1^2 + 2\Gamma_1 \Gamma_2 + \Gamma_2^2) + 2\Gamma_2 \Omega_1^2 (\Gamma_1 + 2\Gamma_2) + \Omega_1^4 \big) + \Gamma_2 \Omega_2^2 (\Gamma_1(3\Gamma_1 + \Gamma_2) + \Omega_1^2) + \Gamma_1 \Omega_2^4 \big) \\
& + \big(\Gamma_2(\Gamma_1 + \Gamma_2) + \Omega_1^2 + \Omega_2^2 \big) \big(\Gamma_1^2 \Gamma_2 + \Gamma_1 \Omega_2^2 + 2\Gamma_2 \Omega_1^2 \big) \big(\Gamma_1 \big(\Gamma_2(\Gamma_1 + \Gamma_2) + \Omega_1^2 \big) + \Omega_2^2 (\Gamma_1 + \Gamma_2) \big).
\end{aligned} \tag{A3}$$

[1] J. F. Clauser and A. Shimony, Rep. Prog. Phys. **41**, 1881 (1978).

[2] A. Aspect, P. Grangier, and G. Roger, Phys. Rev. Lett. **47**, 460 (1981).

[3] A. K. Ekert, Phys. Rev. Lett. **67**, 661 (1991).

[4] D. Bouwmeester, J.-W. Pan, K. Mattle, M. Daniell, A. Zeilinger, and H. Weinfurter, Nature (London) **390**, 575 (1997).

[5] D. Boschi, S. Branca, F. De Martini, L. Hardy, and S. Popescu, Phys. Rev. Lett. **80**, 1121 (1998).

[6] D. C. Burnham and D. L. Weinberg, Phys. Rev. Lett. **25**, 84 (1970).

[7] P. G. Kwiat, K. Mattle, H. Weinfurter, A. Zeilinger, A. V. Sergienko, and Y. Shih, Phys. Rev. Lett. **75**, 4337 (1995).

[8] C. Kurtsiefer, M. Oberparleiter, and H. Weinfurter, Phys. Rev. A **64**, 023802 (2001).

[9] C. E. Kuklewicz, F. N. C. Wong, and J. H. Shapiro, Phys. Rev. Lett. **97**, 223601 (2006).

[10] F. Wolfgramm, X. Xing, A. Cerè, A. Predojević, A. M. Steinberg, and M. W. Mitchell, Opt. Express **16**, 18145 (2008).

[11] J. Fekete, D. Rielander, M. Cristiani, and H. de Riedmatten, Phys. Rev. Lett. **110**, 220502 (2013).

[12] J. S. Neergaard-Nielsen, B. M. Nielsen, B. M. Nielsen, H. Takahashi, A. I. Vistnes, and E. S. Polzik, Opt. Express **15**, 7940 (2007).

[13] A. Haase, N. Piro, J. Eschner, and M. W. Mitchell, Opt. Lett. **34**, 55 (2009).

[14] G. Schunk, U. Vogl, F. Sedlmeir, D. V. Strekalov, A. Otterpohl, V. Averchenko, H. G. L. Schwefel, G. Leuchs, and C. Marquardt, J. Mod. Opt. **2016**, 1 (2016).

[15] D. A. Braje, V. Balić, S. Goda, G.-Y. Yin, and S. E. Harris, Phys. Rev. Lett. **93**, 183601 (2004).

[16] D. N. Matsukevich, T. Chanelière, M. Bhattacharya, S.-Y. Lan, S. D. Jenkins, T. A. B. Kennedy, and A. Kuzmich, Phys. Rev. Lett. **95**, 040405 (2005).

[17] J. F. Chen and S. Du, Front. Phys. **7**, 494 (2012).

[18] B. Srivathsan, G. K. Gulati, B. Chng, G. Maslennikov, D. N. Matsukevich, and C. Kurtsiefer, Phys. Rev. Lett. **111**, 123602 (2013).

[19] G. K. Gulati, B. Srivathsan, B. Chng, A. Cerè, D. Matsukevich, and C. Kurtsiefer, Phys. Rev. A **90**, 033819 (2014).

[20] B. Srivathsan, G. K. Gulati, A. Cerè, B. Chng, and C. Kurtsiefer, Phys. Rev. Lett. **113**, 163601 (2014).

[21] G. K. Gulati, B. Srivathsan, B. Chng, A. Cerè, and C. Kurtsiefer, New J. Phys. **17**, 093034 (2015).

[22] V. Leong, S. Kosen, B. Srivathsan, G. K. Gulati, A. Cerè, and C. Kurtsiefer, Phys. Rev. A **91**, 063829 (2015).

[23] V. Leong, M. A. Seidler, M. Steiner, A. Cerè, and C. Kurtsiefer, Nat. Commun. **7**, 13716 (2016).

[24] T. Chanelière, D. N. Matsukevich, S. D. Jenkins, T. A. B. Kennedy, M. S. Chapman, and A. Kuzmich, Phys. Rev. Lett. **96**, 093604 (2006).

[25] B. R. Mollow, Phys. Rev. **188**, 1969 (1969).

[26] C. Cohen-Tannoudji, J. Dupont-Roc, and G. Grynberg, Optical bloch equations, *Advances in Cryptology - Proc. Eurocrypt'94* (Wiley-VCH Verlag GmbH, Berlin, 1994), pp. 353–405.

[27] R. M. Whitley and C. R. Stroud, Jr., Phys. Rev. A **14**, 1498 (1976).

[28] S. V. Lawande, R. R. Puri, and R. D'Souza, Phys. Rev. A **33**, 2504 (1986).

[29] M. J. McDonnell, D. N. Stacey, and A. M. Steane, Phys. Rev. A **70**, 053802 (2004).

[30] H. H. Jen, J. Phys. B **45**, 165504 (2012).

[31] M. Weber, J. Volz, K. Saucke, C. Kurtsiefer, and H. Weinfurter, Phys. Rev. A **73**, 043406 (2006).

[32] R. T. Willis, F. E. Becerra, L. A. Orozco, and S. L. Rolston, Phys. Rev. A **82**, 053842 (2010).

[33] D.-S. Ding, Z.-Y. Zhou, B.-S. Shi, X.-B. Zou, and G.-C. Guo, Opt. Express **20**, 11433 (2012).

[34] M. Gross and S. Haroche, Phys. Rep. **93**, 301 (1982).

[35] A. D. Tranter, H. J. Slatyer, M. R. Hush, A. C. Leung, J. L. Everett, K. V. Paul, P. Vernaz-Gris, P. K. Lam, B. C. Buchler, and G. T. Campbell, arXiv: 1805.00654.

[36] H. Takesue and K. Shimizu, Opt. Commun. **283**, 276 (2010).

[37] C. Xiong, G. D. Marshall, A. Peruzzo, M. Lobino, A. S. Clark, D. Y. Choi, S. J. Madden, C. M. Natarajan, M. G. Tanner, R. H. Hadfield, S. N. Dorenbos, T. Zijlstra, V. Zwiller, M. G. Thompson, J. G. Rarity, M. J. Steel, B. Luther-Davies, B. J. Eggleton, and J. L. O'Brien, Appl. Phys. Lett. **98**, 051101 (2011).

[38] R. H. Dicke, Phys. Rev. **93**, 99 (1954).

[39] A. V. Akimov, E. O. Tereshchenko, S. A. Snigirev, A. Y. Samokotin, A. V. Sokolov, and V. N. Sorokin, Quantum Electron. **40**, 139 (2010).

6